Engineering of plasmonic gold nanocrystals through pulsed laser irradiation

Guillermo González-Rubio[1,*] and Wiebke Albrecht[2,*]

[1] Physical Chemistry, Department of Chemistry, University of Konstanz, Universitätsstraße 10, D-78465 Konstanz, Germany

[2] Department of Sustainable Energy Materials, AMOLF, Science Park 104, 1098 XG Amsterdam, The Netherlands

* Authors to whom correspondence should be addressed: Guillermo González-Rubio, guillermo.gonzalez-rubio@uni-konstanz.de; Wiebke Albrecht, w.albrecht@amolf.nl

ABSTRACT

Gold nanocrystals (NCs) have drawn tremendous interest in the scientific community due to their unique ability to interact with light. When irradiated with ultrafast pulsed lasers, the lattice temperature of gold NCs can rapidly increase, even above the melting and evaporation thresholds, which results in strong morphological, structural, and aggregation state modifications. Thereby, ultrafast pulsed laser irradiation can lead to the formation of metastable gold nanostructures with distinctive physicochemical features. In this Perspective, we discuss the implementation of femtosecond and nanosecond pulsed lasers to engineer gold NCs. We underline the importance of controlling the heating and cooling dynamics to achieve desired reshaping and restructuring of gold NCs at temperatures below and above its melting point. In addition, we demonstrate the need for advanced electron microscopy characterization techniques and single-particle studies to understand the detailed atomistic mechanisms behind the modifications following pulsed laser irradiation. Finally, we provide our view of the evolving opportunities of ultrafast laser irradiation as a unique tool for the fabrication of unprecedented nanomaterials and catalysts, from metal and multimetal NCs to semiconductors.

INTRODUCTION

The fascinating phenomenon of light-matter interaction has fundamental implications in physics, chemistry, biology, and medicine and is particularly important for enabling next-generation light-harvesting technologies crucial for solving the energy crisis and mitigating climate change. One striking example is the discovery of surface plasmons in metallic films, a phenomenon resulting from the coherent oscillation of the metal's free electrons at the interface with a dielectric in response to an external electromagnetic field.[1–4] This discovery has led to the whole field of plasmonics and opened exciting possibilities in optics, solar harvesting, catalysis, sensing, and medicine.[5–8] In this scenario, the evolvement of nanoscience has added to that fascination because the size confinement of matter to the nanoscale has completely changed our understanding of the light-matter interplay for uncountable material types. For instance, by decreasing the size of a metal object to dimensions below that of the incident electromagnetic radiation wavelength, efficient absorption and scattering of light occur due to the formation of localized surface plasmon resonances (LSPRs).[9] The related high optical cross sections can even exceed the geometrical size of the NCs, leading to strong local electromagnetic field enhancements at the NC surface with the confinement of light to volumes of a few tens of nm^3. Out of different plasmonic metals such as copper or silver, gold NCs have attracted particular attention due to their ease of synthesis, high chemical stability, low toxicity, and morphological tunability.[5–8,10] As the optical resonances are closely linked to the NC's morphology, shape engineering provides unique possibilities to precisely tune their optical properties. For instance, gold nanorods (NRs) display two LSPR modes associated with their transversal and longitudinal dimensions. By increasing the aspect ratio (ρ, ratio between the NR length and width), the longitudinal LSPRs can be finely tuned from ca. 600 nm to above 2000 nm [9,11–13]

In 1974, the understanding of light-matter interactions was significantly accelerated thanks to the experimental demonstration of the first light amplification by stimulated emission of radiation (laser) device with pulses in the femtosecond scale.[14] In the field of plasmonics, this technology was crucial for investigating the excitation and relaxation dynamics of LSPRs in metallic, particularly gold, nanostructures.[15–17] The combined findings revealed that during ultrafast laser irradiation, the kinetic energy of free electrons rapidly increases in less than 100 fs due to the absorption of the photon energy (Figure 1). This process is followed by thermal equilibration of the electron energy via electron-electron scattering in a few tens of fs and then by the energy transfer to the lattice via electron-phonon coupling in a few ps. Finally, thermal equilibrium between the NC lattice and the surrounding is reached at time scales ranging from tens to hundreds of ps. Due to the energy transfer to the NC lattice, its temperature can significantly increase before heat dissipation to the environment cools it down again, even reaching temperatures above melting (i.e., 1337 K) and boiling (i.e., 2973 K) points. Consequently, such a photothermal process can cause temperature spikes that result in unique structural and morphological NC changes, not achievable via standard heating methods.[15–26] This fact is particularly true for anisotropic NCs, where the adsorbed laser pulse energy triggers the reduction of the NC anisotropy to more spherical morphologies with reduced surface free energy (i.e., thermodynamically favored shapes).[21,22,25,27–30] Moreover, compared with continuous wave laser excitation, the peak power of a pulsed laser is much higher

(10^7–10^{12} W/cm^2 vs 10^4–10^6 W/cm^2), which explains the more significant impact of ultrafast pulsed laser excitation on NC size, morphology and crystalline structure.[31,32]

Mechanistic understanding of the structural and morphological changes is important to either prevent or guide single NC modifications. Most excitingly, it is possible to take advantage of the fast heating and cooling processes underlying ultrafast pulsed laser excitation to develop completely different NC synthetic pathways. Indeed, NC shapes, unattainable from the standard colloidal synthesis routes, can be created with ultrafast laser pulses due to the involved highly out-of-equilibrium processes. Together with the observations that reshaping even occurs hundreds of degrees below the bulk melting temperature,[29,33–39] getting better control over reshaping and restructuring processes has fueled researcher's interest in understanding their underlying physical principles and kinetic pathways.

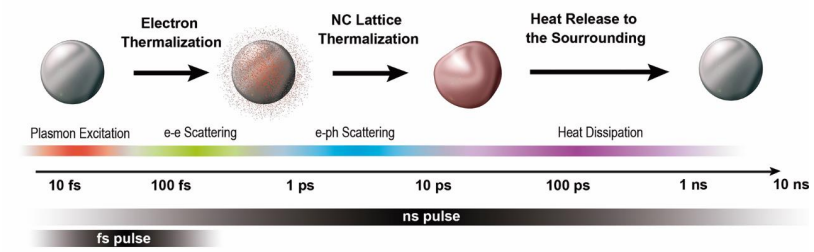

Figure 1. Ultrafast pulsed laser irradiation-induced heating of gold NCs via the photothermal mechanism. After irradiation, the metal's electrons (either interband or conduction band electrons) are excited and thermalized in less than 500 fs via electron-electron coupling. The NC's lattice is subsequently thermalized through electron-phonon coupling, giving rise to melting and possibly fragmentation (if sufficient energy has been deposited). The heat is finally released to the environment, and the NC cools down to the surrounding temperature again. For fs-laser excitation, these processes happen consecutively. In the case of ns-pulses, the heating and relaxation processes coincide.

In this Perspective, we focus on the implementation of femtosecond and nanosecond pulsed lasers to govern the morphological, aggregation state, structural and plasmonic features of colloidal gold NCs, with emphasis on our contributions to the research field. The ability of ultrafast laser pulses to reshape and restructure gold NCs is discussed, pointing to the importance of controlling the cooling dynamics as a critical aspect of control over such processes. In this context, the contributions of advanced electron microscopy characterization techniques and single-particle studies are critical for studying the structural modifications occurring on the NC lattice after pulsed laser irradiation. We first describe the mechanistic insights that have so far been gained in the reshaping and restructuring process of gold NCs. Afterward, we present examples of nanostructures that can be created by controlled femtosecond and nanosecond pulsed laser excitation of gold NCs. The last section aims at providing future research directions, emphasizing the potential of laser irradiation for the synthesis of advanced metal-based catalysts and the need for *in situ* characterization techniques.

HEATING AND COOLING RATES

The morphological fate of the irradiated NCs is directly dependent on the rate of energy deposition (laser pulse length and fluence), as compared to the relaxation dynamics (electron-phonon and phonon-phonon interactions with the environment), as well as the initial particle morphology (Figure 2a-d) as the lattice temperature that can be reached within the gold NC heavily depends on these parameters. The NC's temperature increase is often calculated with the two-temperature model, where the electronic temperature T_e, lattice temperature T_l and surrounding medium temperature T_m are determined via coupled differential heat equations.[40] For femtosecond laser excitation, i.e. excitation that is faster than the electron-phonon coupling time, the laser pulse energy is absorbed by the electronic system resulting in high electronic temperatures (Figure 2e left side). In this case, electronic absorption, heat transfer to the NC lattice and surroundings can be considered to happen successively and the NC lattice temperature increase δT is linearly dependent on the pulse fluence F:[41]

$$\delta T = \frac{\sigma_{abs} F}{V \rho c_p} \quad (1)$$

where σ_{abs} and V are the absorption cross section and volume of the NC, respectively, and $V\rho c_p$ is its total (lattice + electronic) heat capacity. As can be seen from eq. 1, next to the laser excitation parameters, the ultimate temperature that can be reached through femtosecond laser excitation also depends on the plasmonic properties of the NC as the temperature increase is proportional to the absorption cross section. In this sense, it is maximal when the NC is irradiated at its LSPR and strongly depends on the shape of the NC. Elongated NCs with high aspect ratios are more efficient 'nano-antennas' compared to spherical NCs and exhibit higher absorption cross sections, resulting in higher temperature increases under laser excitation (given that the excitation wavelength matches the plasmon peak).[42,43] Consequently, higher fluences are needed to reshape spherical-like NCs (Figure 2d) compared to anisotropic NCs (Figure 2a-c). For nanosecond irradiation, the laser pulse excitation is much longer than the heat transfer to the lattice and a quasi-thermal equilibrium of T_e and T_l is established (Figure 2e right side).

The resulting reshaping and fragmentation processes are consequently also significantly influenced by the laser pulse width and fluence. Because in gold NCs electron-phonon scattering happens at time scales in the picosecond regime, their excitation with femtosecond laser pulses can lead to sharp lattice temperature increases (Figure 2e). However, as the cooling rate is also fast (in the ps-ns range), the effective heating time is only a few ps (Figure 2f). This short heating time restricts the available time for atoms to diffuse (e.g., limiting the aspect ratio change of the NR shown in Figure 2f). Therefore, reshaping is less as it would be for longer pulses, e.g. nanoseconds, given that the same peak temperature would be reached.[43] Consequently, the lattice temperatures typically required for reshaping are higher than those needed under standard heating experiments (e.g. external heating in a furnace or oven), for which the heating time is much longer. For instance, NRs heated with fs laser pulses to a temperature of 700°C did not show morphological changes but deformed completely to spherical-like NCs at 250°C in an oven for 1 hour.[29] However, higher fluences are needed for nanosecond pulse excitation to reach the same peak temperatures as for femtosecond laser experiments. The reason is that the increase of the pulse duration, as in the case of nanosecond pulsed laser

irradiation, implies that photothermal heating and cooling processes coincide, making heating less efficient. Therefore more energetic pulses are required to produce reshaping effects.[19,44]

As opposed to reshaping, fragmentation processes are even more intricately linked to the pulse length and fluence as non-thermal processes such as Coulomb repulsion can contribute. This is particularly true for femtosecond pulse irradiation. One potential explanation is the extreme near-field enhancement occurring close to the NC surface after excitation with an fs-laser pulse, which could trigger NC fragmentation even below the melting point of gold.[45,46] If thermionic emission of electrons and photothermal melting take place simultaneously, highly charged droplets can be formed and eventually break up into smaller ones due to Coulomb instability.[40,47–49] Simulations revealed that for gold NCs of 54 nm in water, a T_e slightly above 7000 K is required to induce such fragmentation effects (Figure 2e).[40] Under nanosecond pulse irradiation, T_e is typically not high enough for Coulomb explosions (Figure 2e). Fragmentation effects during ns-pulse laser experiments are therefore often ascribed to a photothermal evaporation mechanism (i.e., the heating–melting–evaporation model), where T_l reaches the boiling temperature of gold (as compared with fs-laser excitation, where the boiling temperature is not reached), leading to surface evaporation.[40,44,50] Nevertheless, fragmentation via Coulomb explosion has also been observed in gold NCs irradiated with nanosecond laser pulses.[51,52] Besides the pulse width and wavelength, the NC's size is also a determining parameter in the fragmentation process as it changes the physical parameters of the NC such as its melting and boiling temperature and plasmonic absorption cross section.[53]

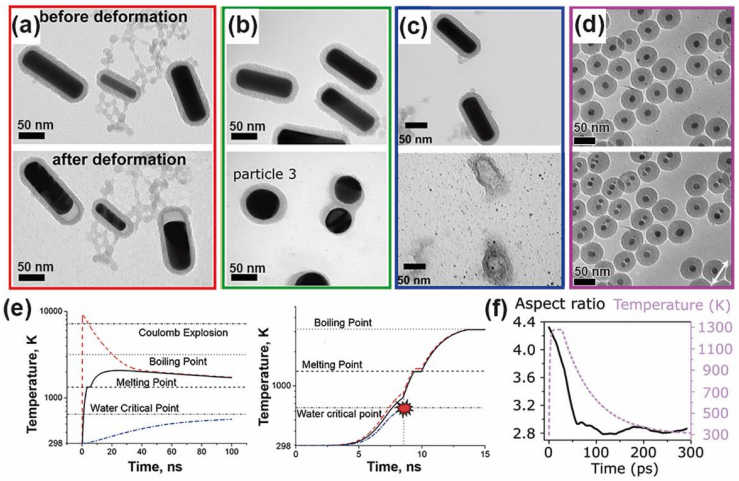

Figure 2: Reshaping and fragmentation of gold NCs excited with fs and ns pulsed laser irradiation. (a-d) Femtosecond laser-induced deformation of single mesoporous silica-coated NRs (a-c) and NSs (d) irradiated at their main LSPR (860 nm for NRs and 515 nm for spherical NCs) with (a) 5.3 mJ/cm^2, (b) 10.6 mJ/cm^2 (c) 13.8 mJ/cm^2 and (d) 22 mJ/cm^2. Depending on the absorbed energy, the NCs can slightly (b) or strongly (b) reshape and (c,d) fragment. It is interesting to note that the plasmonically less efficient spherical NCs require a higher fluence to fragment compared to the NRs, which is a result of their lower absorption cross section. A

double-headed arrow indicates the polarization in (d). (a-c) Modified with permission from Nano Lett., 16, 1818–1825 (2016). Copyright © 2016 American Chemical Society. (d) Modified with permission from ACS Nano, 13, 12445–12451 (2019). Copyright © 2019 American Chemical Society. (e) Calculated evolution of T_e (red dashed curve), T_l (black solid curve), and T_m (at the NC−water interface, blue dashed-dotted curve) due to excitation with: (left) 300 fs at 400 nm and a fluence of 10 mJ/cm^{-2} and (right) 5 ns at 355 nm and fluence of 28 mJ cm^{-2}. Commence of the surrounding water vaporization (at the NP-water interface) is represented by the explosion symbol. Modified with permission from J. Phys. Chem. C, 115, 5063–5072 (2011). Copyright © 2016 American Chemical Society. (f) Simulated lattice temperature (magenta curve) of a gold NR upon excitation with a 140 fs laser pulse and the correlated reshaping of the NR (evidenced by its aspect ratio change), which was simulated by molecular dynamics simulations. Due to the short heating time upon fs laser excitation, the available short time for atomic diffusion limits the reshaping process. The simulations were performed on the same NR as discussed in detail in Figure 4. Reproduced with permission from Adv. Mater., 33, 2100972 (2021) Copyright 2021 Wiley-VCH GmbH.

These results evidence the fact that the excitation and relaxation dynamics of plasmonic gold NCs excited with ultrafast pulsed laser irradiation are strongly determined by the interplay between many parameters, including pulse width and fluence, irradiation wavelength, NC size, and the surrounding environment. In practice, initial investigations typically showed insufficient control over the shape and size dispersions of the products, which impaired their systematic implementation in colloidal gold NC syntheses.[19,20,22,54]. This fact could be partially explained by the lack of understanding of the role of surface ligands in the cooling dynamic and reshaping process. It is important to note that colloidal gold NCs are portions of gold crystals with dimensions typically below 100 nm (although those with sizes between 100 and 300 nm are often included in this category) and are dispersed in a medium such as water, toluene, or hexane. In order to maintain their colloidal stability (i.e., avoid their uncontrolled aggregation),[55] it is necessary to screen the attractive Van der Waals interactions between NCs (due to transient fluctuations in the electron distributions). Colloidal stabilization is typically provided through organic ligands attached to the gold NC surface that can effectively impart repulsive interactions via steric or electrostatic interactions.[55–57] In the case of gold NCs, cetyltrimethylammonium bromide (CTAB) and polyethyleneglycol (PEG) are often utilized to stabilize them in water, while oleylamine and polystyrene are used to gain stability in organic solvents.[58–62] Colloidal stability can also be achieved via inorganic coatings, such as silica.[63,64]

In most cases, surface ligands possess lower thermal conductivity and heat capacity than water (i.e., the solvent often used to investigate the effect of pulsed laser irradiation on colloidal gold NCs; 0.5984 W m^{-1} K^{-1} and 4.1742 J cm^{-3} K^{-1} at 20ºC),[65] slowing down the heat transfer to the environment. For instance, investigations on the cooling dynamics of gold NRs coated by CTAB layers showed that the heat capacity of the surfactant layer is 2.0 ± 0.3 J cm^{-3} K^{-1}. Moreover, the thermal conductivity of the surfactant layer was found to decrease from 0.24 to 0.18 W m^{-1} K^{-1} when the CTAB concentration increased above the critical micelle concentration (cmc), which implies that the cooling process is delayed when the CTAB concentration is raised.[66] When layer-by-layer polyelectrolyte coatings were used for colloidal stabilization, an increase in the thermal conductivity and heat capacity was observed compared to CTAB, probably due to greater water penetration into such a polyelectrolyte shell. However, the opposite effect was measured after the

growth of a mesoporous silica shell around the gold NRs, as the lower thermal conductivity of the silica compared to that of CTAB delayed the cooling process.[67] In addition, a thinner mesoporous silica shell resulted in slower heat dissipation compared to a thicker shell, which was attributed to an additional interfacial resistance at the silica-water interface. Overall, these results point to the role of surface ligands and coatings on the cooling dynamics and the potential of controlling it through the interplay between the nature and thickness of the surface ligand shell or coating. Such parameters could be experimentally maneuvered, for instance, by the concentration of surfactant, [66] the molar mass of the surface ligand[68] (e.g., polymer chains of higher molecular mass can lead to thicker shells), or the grafting density on the NC surface[69] (e.g., through increasing the concentration of surface ligand during the NC surface functionalization process). It should be noted that surface ligands and coatings also play a role in surface atom mobility, which will be discussed further below.

Based on the initial insights, a remarkable example of control provided by heat dissipation engineering on the reshaping process was shown for the case of CTAB-stabilized gold NRs. At the optimal CTAB concentration, we obtained colloidal solutions with exceptionally narrow LSPR bands via femtosecond laser pulse reshaping (Figure 3a).[25] The procedure consisted of irradiating gold NRs with an initial aspect ratio ρ_0=3.87 and a longitudinal LSPR band located at 800 nm, i.e., the wavelength of the 50-fs-pulsed Ti:sapphire laser utilized for the reshaping experiments. In the presence of 1 mM CTAB (at the cmc), femtosecond irradiation for 1 hour at a fluence of 0.32 mJ/cm^2 led to a prominent blue-shift of the LSPR band of ~70 nm. Most remarkably, an increase of the maximum intensity was distinctly noted, as well as a significant reduction of the full width at half maximum (FWHM) from 0.24 to 0.09 eV, which nearly matched the 0.07 eV calculated for a single NR with the average dimensions of the NRs after reshaping (Figure 3e). The change in the optical properties was explained by the reduction of the NR average aspect ratio from 3.6 ± 0.5 to 3.00 ±0.05 (Figure 3b,c). MD simulations conducted to gain insight into the interaction of CTAB with the gold surface revealed, that at the cmc, partial surface coverage by small micelles occurred (Figure 3d). As a result, a significant fraction of the gold surface was still in close contact with water molecules, which seemed to favor optimal heat transfer and NR cooling. However, uncontrolled reshaping was observed when the NR laser irradiation was performed in higher CTAB concentrations, as indicated by the resulting asymmetric LSPR band (Figure 3e). Investigations on the time constant of the heat transfer process from gold NRs to water have shown that the heat transfer time constant, τ, is close to 60 ps, while for CTAB at concentrations around the cmc, τ ~ 350 ps[28]. MD investigations revealed that this slower cooling rate (τ ~ 350 ps) was critical to achieving a gentle reshaping of the gold NRs, as it gives them just the right amount of time at elevated temperatures for reshaping (Figure 3f). When using the relaxation dynamics related to water, τ ~ 60 ps, too fast heat transfer to the surrounding lead to minor deformations.

The observed LSPR band narrowing was also attributed to a self-limiting multishot process: once the NRs reached the final aspect ratio, their resonances shifted out of the excitation window, and the NRs did not absorb enough energy anymore to reshape further. The normalized variation of the aspect ratio, $\Delta = (\rho_0 - \rho)/(\rho_0 - 1)$ (i.e., independent of the initial aspect ratio) depends on the energy deposited by a laser pulse, which varies with (i) the absorption cross-section at the laser wavelength (i.e., that depends on ρ) and

(ii) the orientation of the NR with respect to the laser polarization. It was found that below ~0.38 eV/atom (in the electronic system), a single pulse could barely modify the NR, while its ability to do so increased dramatically above that energy threshold. Increasing the energy deposited on the NR using higher pulse fluences to accelerate the reshaping process led to heavily modified NRs with ϕ-shaped morphology (at energies between 0.38 and 0.49 eV/atom, and temperatures up to ca. 1900 K) and spheres within a single pulse, effects that were also observed in the MD experiments (Figure 3g) and in earlier works as well.[70]. Overall, the gentle NR reshaping was hence dependent on the pulse fluence, the concentration of surfactant, and the NR aspect ratio. Moreover, NRs with higher aspect ratios underwent a faster reshaping due to their lower thermodynamic stability.[39] These effects eventually directed the emergence of a higher fraction of NRs with similar aspect ratios, leading to the described narrowing of the LSPR bands of the whole ensemble. Thus, next to the influence of the plasmonic properties on the reshaping process (see discussion above), the opposite is also true: reshaping can control the plasmonic properties.

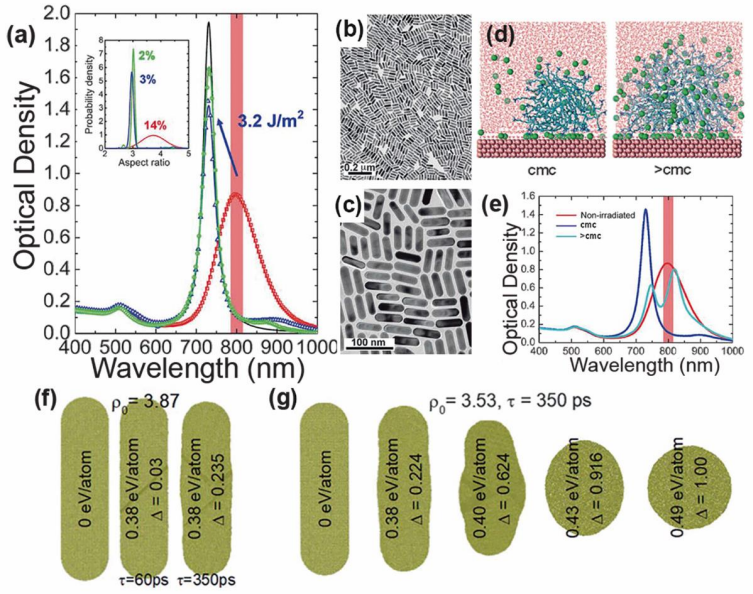

Figure 3: Reshaping of gold NRs under fs pulsed laser excitation. Femtosecond laser-reshaping of CTAB-stabilized (at the cmc) gold NRs (e, red) using 0.32 mJ/cm^2, 800 nm 50-fs pulses (a, red vertical band) yields NRs with ultranarrow LSPRs (a, blue). After the removal of spherical impurities, the spectra of the reshaped NRs nearly match the calculated one for a single NR (a, green). The symbols represent the experimental optical density spectra, while the lines are the fitted optical density spectra. The black line represents the calculated spectra of a single gold NR. (b and c) Representative TEM images of irradiated gold NRs. (d) MD simulations performed on an Au (100) surface (d, red spheres) suggest the adsorption of CTAB micelles (d; CTA^+, bromide ions, and water molecules are represented by blue, green, and red sticks, respectively) with different dimensions depending on the CTAB concentration (at or

above the cmc), which would affect the cooling process and explain the distinct reshaping effects observed on the gold NRs (e, red) irradiated at CTAB concentrations of 1.0 mM (e, blue) and 5.0 mM (e, cyan). (f,g) MD simulations of gold NRs' aspect ratio evolution after excitation with a fs-laser pulse depending on (f) the thermal insulation provided by water: $\tau \sim 60$ ps and CTAB at the cmc $\tau \sim 350$ ps; and the (g) total deposited energy by the laser pulse. Reproduced with permission from Science. 368, 1472–1477 (2020) Copyright 2017 AAAS.

ATOMISTIC-SCALE MECHANISMS

Although pulsed laser excitation can heat gold NCs above their melting point, reshaping and restructuring have also been observed at hundreds of degrees below it, either under low fluence (cw or pulsed) laser excitation or thermal heating.[29,34–39,71] For example, gold NRs and nanostars were shown to strongly reshape at external heating temperatures as low as 200 °C in a few minutes.[35,38] These below-melting-point morphological changes have triggered several studies trying to explain the reshaping phenomena at the atomic level. In the early works on the pulsed laser-induced reshaping of gold NRs, Link and co-workers proposed a crystal defect-driven mechanism based on the observation of crystalline point and line lattice defects in the NCs after pulsed laser excitation.[21] The reshaping was suggested to start with the creation of internal point defects, which could subsequently grow into twinning and stacking faults through local melting and simultaneous surface diffusion. This process could be driven by the transformation of {110} into more energetically favorable {100} and {111} surface facets.

In 2014, Taylor et al. measured the aspect ratio of single gold NRs before and after femtosecond laser excitation by transmission electron microscopy (TEM).[39] To their surprise, not the NRs in laser-resonance condition (in terms of wavelength and polarization direction) reshaped most but the degree of reshaping was strongly dependent on the initial aspect ratio. The authors attributed this phenomenon to a curvature-driven surface diffusion process stemming from the chemical potential difference between high and low curvature regions. Thereby, it was possible to explain the stronger reshaping suffered by high aspect ratio NRs, (i.e., more strongly out-of-equilibrium NRs) and the higher activation energies needed to modify NRs of low aspect ratio. It was found that the activation energy for surface diffusion varied from 1.5 eV to 0.6 eV when increasing ρ from less than 3 to 5. The proposed curvature-driven diffusion mechanism was confirmed by *in situ* electron tomography experiments performed on gold nanostars and gold-palladium octopods under thermal heating conditions.[33,38] However, recent additional *in situ* heating experiments performed inside the transmission electron microscope questioned whether such a mechanism is valid for every anisotropic NC shape.[72] The authors argued that the actual pathway was determined by the initial shape of the NC. Thus, whereas a gold NR deformed via a curvature-driven mechanism, a nanotriangle reshaped via surface faceting through a layer-by-layer migration of vertex atoms to the triangular faces. In addition, no signs of crystal defects were found in such experiments.

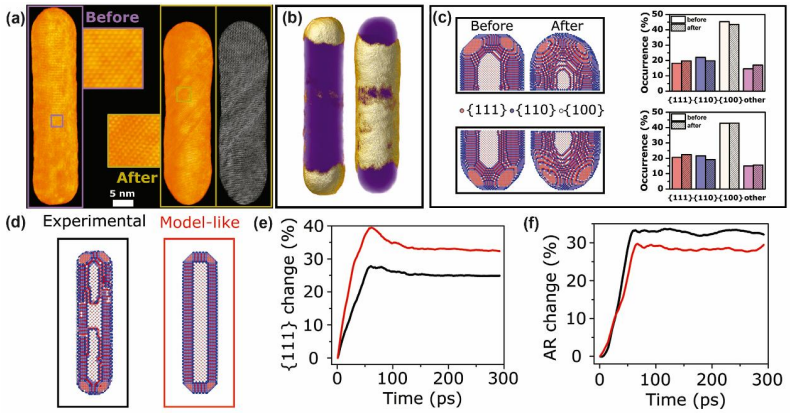

Figure 4: Atomic resolution tomography of the same silica-coated gold NR before and after femtosecond laser excitation. (a) 3D visualization of the reconstructed gold NR before and after excitation with multiple femtosecond laser shots (925 nm, 6.5 mJ cm^{-2}) along the same viewing direction. Whereas the NR was single-crystalline before laser excitation (left box), it contained multiple twinning defects afterward (right boxes). (b) Upon laser excitation atoms redistributed from the tips (golden color left side) to the sides (golden color right side) of the NR. (c) Visualization and quantification of the facet distribution at the two tips before and after laser excitation. (d-f) MD results of the (e) relative change in {111} facets and (f) aspect ratio change for two different NRs of the same volume and aspect ratio, either based on the synthesized silica-coated gold NR (black curves) or on a model-like NR (red curves). Reproduced with permission from Adv.Mater., 33, 2100972 (2021) Copyright 2021 Wiley-VCH GmbH.

To disentangle these seemingly contradictory observations, we need to start by looking at the differences in time scales and the interplay between thermodynamics and kinetics. Thermal heating experiments, such as the *in situ* experiments inside the TEM, are performed at time scales ranging from seconds to minutes or even hours, where there is enough time for atoms to diffuse in an optimal way to reach more thermodynamically stable sites (i.e., those of lower free energy). On the contrary, heating under pulsed laser irradiation occurs at ultrashort time scales. As mentioned in the previous section, under ultrafast heating and cooling induced by pulsed laser irradiation, gold NCs did not remain hot for long enough, and higher temperatures were therefore required to achieve an identical reshaping occurring during thermal heating processes.[29] Moreover, the ultrashort heating and cooling times result in kinetically trapped structures (i.e., metastable states), explaining the observation of atomic lattice crystal defects after pulsed laser excitation.

In this scenario, shedding light on the kinetic processes demands experiments with an ultrafast time resolution that can be carried out on a single metal NC and with the sufficient three-dimensional resolution to characterize such processes at the atomic level. We have recently addressed this challenge by performing atomically resolved electron tomography before and after femtosecond laser excitation on the same single mesoporous silica-coated gold NR (Figure 4a) and using the measured atomic positions for MD simulations to extract the missing temporal evolution.[43] Electron tomography was hereby crucial to reliably resolve the 3D morphology and surface facets without any assumptions

about the otherwise hidden third dimension. In electron tomography, a series of 2D projection images of the same object from different directions is used to reconstruct the 3D shape and interior of the object. However, contrary to computed tomography, which normally covers the full ± 90 ° angular range needed for the best reconstruction, electron tomography is often limited to an angular range of about ± 75 °. The reason is that the space in-between the objective lens' pole pieces in a TEM, where the sample holder is inserted, is restrained to a few millimeters leaving little space for tilting the holder. The resulting missing angular information is referred to as the 'missing wedge', and it can create artifacts that can be minimized by applying advanced reconstruction algorithms and machine learning.[73,74] A significant obstacle of electron tomography is the limited temporal resolution one can achieve for *in situ* processes, as the acquisition of one tomography series takes around 30-60 minutes. Although approaches exist to speed up the acquisition significantly,[75] ultrafast non-reversible processes such as pulsed laser-induced reshaping are still beyond the realm of what is currently achievable. Nonetheless, fast electron tomography has contributed to unraveling thermally induced diffusion processes.[76]

In this context, the extension of electron tomography to the atomic scale has been tremendously important for our research interest,[77–80] as it allowed us to quantify the number of atoms diffusing under femtosecond pulsed laser excitation, identify the formed lattice defects and their distribution inside the NR, and determine the ratio of surface facets before and after the NR reshaping.[43] Thereby, we observed that multishot femtosecond laser irradiation at the longitudinal LSPR (925 nm, 6.5 mJ cm^{-2}) promoted the diffusion of 28000 atoms from the tips of the NR to its sides (Figure 4b). At the same time, twin boundaries appeared after the laser excitation, which extended throughout the whole initially defect-free mesoporous silica-coated gold NR (Figure 4a). In addition, the fraction of {111} surface facets increased while that of the less stable {100} and {110} facets decreased (Figure 4c). Furthermore, by using the retrieved atomic-scale morphology of the gold NR before laser excitation and mimicking the laser-induced heating computationally, molecular dynamics simulations enabled us to unravel the underlying atomic processes with ultrafast time resolution. Thereby, we noticed that the immediate onset of surface diffusion simultaneously caused the reduction in aspect ratio and facet restructuring. Then, the combination of localized stress propagating from the surface through the internal structure with the confined melting around internal lattice defects was found responsible for the formation of internal stacking faults, which subsequently grew into parallel multitwin boundaries under continuous shear strain. It is important to note that these processes were strongly dependent on:

- *The mesoporous silica shell*: It significantly improved the morphological stability of the irradiated gold NR. On the one hand, it physically hindered gold atom diffusion. On the other hand, it slowed down heat dissipation, leaving the NR just a little bit more time to recrystallize into its FCC structure with multitwin boundaries, for which it did not have to pay a high energetic penalty. Heat dissipation of uncoated gold NRs was faster, resulting in energetically less favorable irregular stacking faults and a partially disordered crystal lattice. Giving the NR orders of magnitude more time at the laser pulse peak temperature resulted in more strongly reshaped defect-free particles. As also pointed out in the previous section, the ratio of heating and cooling

times thus radically impacted the final morphology and internal structure of the irradiated gold NC.

- *The atomic arrangement of the initial NR.* It influenced the final morphology and kinetic pathway, a fact which was recognized by comparing the results obtained on the experimental gold NR morphology to a model NR of the same volume and aspect ratio but without any surface disorder (Figure 4d). In the latter case, fewer {111} surface facets were initially present, resulting in a more remarkable change in the surface faceting to increase the amount of {111} facets (Figure 4e). Nonetheless, the model-like NR was more stable as no kinks or steps were present at the surface to facilitate surface atom diffusion processes (Figure 4f).

Overall, our results show that all below-melting point reshaping mechanisms reported in the literature are linked and probably occur simultaneously. Moreover, the exact reshaping and restructuring pathways are strongly dictated by the interplay of heating and cooling rates and the exact atomic-scale morphology of the initial NC.

OUT-OF-EQUILIBRIUM NANOCRYSTALS

A detailed understanding of the importance of heating and cooling rates, including the underlying reshaping mechanism of gold NCs, shall eventually allow for rational control over the formation of distinct kinetically trapped nanostructures, i.e., metastable or out-of-equilibrium NCs. A remarkable example is hollow gold NCs created from spherical NCs upon nanosecond pulsed laser excitation.[24] NCs with cavities have drawn significant attention due to their potential as drug carrier nanomaterials for diagnosis and treatment in biomedicine.[81,82] In our work, careful control over the interplay between pulse fluence and surfactant concentration was necessary to create hollow NCs. Specifically, 20 nm gold nanospheres with LSPRs centered at 523 nm were irradiated with 532 nm 8 ns laser pulses at a fluence of 200 mJ/cm^2. The efficient formation of cavities was achieved in the presence of 25 mM CTAC, which was accompanied by a reduction of the average NC size to 16 nm (Figure 5a-d). The critical role of a specific heating-to-cooling ratio was evident in control experiments where different morphologies were obtained depending on the fluence, CTAC concentration, or NC size.

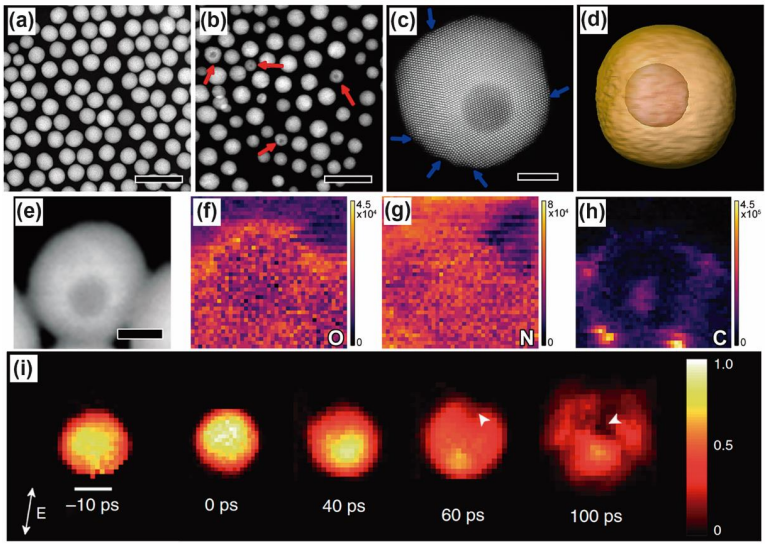

Figure 5: Laser-induced cavity creation in spherical gold NCs. (a) and (b) display low magnification scanning TEM (STEM) images of gold NCs before and after irradiation with 8 ns laser pulses at a wavelength of 532 nm (fluence of 200 mJ/cm^2, repetition rate of 10 Hz), respectively. Size reduction and cavity creation (marked in red) were observed. (c) Atomic resolution STEM image of a gold NC containing a cavity. Blue arrows indicate twin planes. (d) Electron tomography visualization of a gold NC with a cavity confirms that the cavity was fully enclosed by the gold NC. Scale bars are 50 nm (a and b) and 4 nm (c). (e) EELS measurements of a NC with a cavity and the corresponding (f) oxygen, (g) nitrogen, and (h) carbon maps. In particular, carbonaceous material was identified inside the cavity. Reproduced with permission from J. Phys. Chem. Lett., 11, 670–677 (2020). Copyright © 2020 American Chemical Society. (i) Time-resolved single-shot diffractive images obtained with X-ray laser pulses show the void formation during melting of a 100 nm gold NC excited with a single 800 nm 50-fs laser pulse at a fluence of 870 mJ/cm^2. The white arrowheads point to the void formation. Reproduced with permission from Nat Commun 10, 2411 (2019). Copyright © 2019, Ihm, Y., Cho, D.H., Sung, D. et al.

The cavity creation mechanism at the optimal heating-to-cooling rate was revealed by a combination of (*in situ*) electron microscopy and MD simulations. It was hypothesized that in nanosecond pulsed irradiation experiments, after gold NC melting occurred, stretching of the liquid droplets led to the emergence of gaps. At sufficiently high energies, a further expansion of the droplet released some fragments (i.e., which could explain the observed average size reduction from 20 to 16 nm). During this process, small amounts of water and organic matter (resulting from the surfactant molecules) likely went inside the gold NC through the created gaps and remained trapped during the recrystallization process (i.e., cooling process), which stabilized the cavity. In this regard, MD simulations showed that the cavity migrated to the nearest surface under thermal heating when it contained trapped matter. However, in the case of empty cavities, thermal heating led to their destabilization and disappearance without migration. By *in situ* heating electron tomography, we could indirectly verify that matter got trapped as we observed cavity migration to the nearest surface at elevated temperatures. In addition,

electron energy loss spectroscopy (EELS) measurements directly confirmed the presence of organic material inside the cavity (Figure 5e-h). Interestingly, the phenomenon of void formation during melting and fragmentation of gold NCs under pulsed laser irradiation has been characterized through time-resolved single-shot diffractive imaging using X-ray laser pulses.[83] Such experiments performed on 100 nm gold NCs excited with 800 nm 50-fs laser pulses allowed to observe the formation of voids after 60 to 100 ps due to the stretching of the melted NC (Figure 5i). This demonstration of hollow nanostructures formation through localized heating could be the first step toward the fabrication of plasmonic nanocarriers on demand.

Another example is the potential for ultrafast laser excitation in self-assembly processes.[26] Self-assembly is a process by which disordered components organize themselves into ordered structures.[84] In the field of gold nanomaterials, it holds tremendous potential for the fabrication of plasmonic nanostructures with unique and enhanced functionalities.[85] The effects induced by ultrafast pulsed laser irradiation on gold NCs can be beneficial in the context of NC self-assembly, where the aggregation process and the nature of the self-assembled structures can be rationally tailored with the help of ultrafast laser pulses.[86] More specifically, we demonstrated that the tip-to-tip assembly of gold NRs with alkyl chain dithiols as molecular linkers and a longitudinal LSPR resonance at 600 nm can be beneficially influenced. Under standard conditions, in the absence of laser irradiation, the self-assembly process resulted in a variety of preferentially tip-to-tip self-assembled NRs ranging from dimers to large chains with more than ten NRs. The yield of targeted dimers could be significantly increased upon irradiating the solution by 0.13 mJ/cm^2 femtosecond laser pulses at 800 nm. The reason lies in the hybridization of plasmonic modes in coupled NCs. For gold NRs with the LSPR band located at 600 nm and assembled into linear aggregates (using 1,8-octanedithiol as molecular linker), a significant redshift of the longitudinal mode occurred, where dimers and trimers absorbed at ca. 700 nm and 800 nm, respectively. Thus, the excitation with 800 nm pulses specifically targeted trimers. The field enhancement inside the gaps between NCs, which can be several orders larger than the incident field,[9,87] led to efficient absorption of the trimers at this wavelength. The subsequent photothermal process resulted in the decomposition of the molecular linkers in trimer structures, inhibiting the formation of trimers and larger aggregates, thereby increasing the relative yield of dimers and monomers.

When the pulse fluence was increased to 0.65 mJ/cm^2, the trimer temperature rose above the threshold for surface diffusion and the decomposition of the molecular linker. Because the atoms at the tips are most mobile (see section above) and because van der Waals forces between gold NCs are strong, tip-to-tip welding of the NRs occurred (Figure 6a-e), leading to plasmonic nanostructures with LSPR bands in the 900 to 1400 nm range (Figure 6f-l). The emergent LSPRs in this range could be attributed to the presence of a conductive nanojunction between the NRs, which permits charge flow between the welded NRs, and is known as the charge transfer plasmon (CTP) mode (Figure 6j-l). Interestingly, the characterization of the 3D (atomic) structure of the welded assemblies by high-resolution electron tomography showed that the welded NCs exhibited a confined crystalline defect at the interface (Figure 6c-e).[88] In the case of crystallographic orientations of the two adjacent NRs, this was a dislocation, whereas grain boundaries formed for those with larger misorientation (Figure 6a-e). The defect creation can be

understood in the light of the discussion of the atomic-scale reshaping mechanism described above, where the ratio between the heating and cooling rate did not allow the kinetically-trapped nanostructures to form a defect-free crystal lattice. The beauty is that pulsed laser excitation allowed for the creation of such an out-of-equilibrium system with one defined lattice defect in the middle, which would not be possible to synthesize by conventional heating routes (i.e., where it is not possible to selectively weld preassembled gold NR dimers over structures formed by a larger number of NRs). As a consequence, this crystallinity engineering can enhance our fundamental understanding. In the case of the welded NRs, we used such structures to explore the influence of a single crystal defect on the plasmonic performance of gold NCs at the single-particle level using EELS.[88] By comparing the welded NRs to single-crystalline NRs at the same resonance energy, we observed a 1.3-1.4 times broadening of the CTP mode compared to the longitudinal LSPR of the single-crystalline NRs. By simulations, we could exclude that this was a shape effect and attributed the plasmon damping to the presence of a *single* crystal defect.

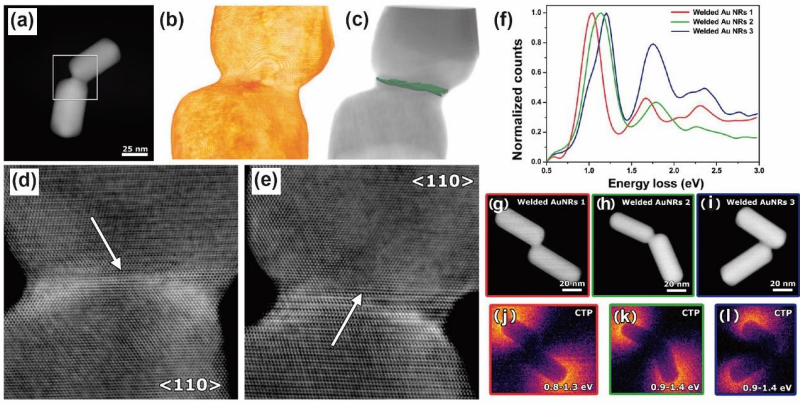

Figure 6: Welding of gold NRs through femtosecond laser excitation. (a) Welded gold NRs after femtosecond laser irradiation at 800 nm with 0.65 mJ/cm^2. Atomic resolution electron tomography was used to investigate the region inside the white box. (b) 3D visualization of the reconstructed atomic resolution electron tomography of the gap region. (c) Segmentation revealed a grain boundary at the interface. (d,e) Orthoslices through the 3D reconstruction, along different orientations, confirming the presence of a grain boundary. The white arrows in (d,e) indicate the plane where the defect is located. (f) Normalized EELS spectra of three different welded NR pairs shown in panels (g−i) reveal a rich landscape of plasmon modes. In particular, at low energies, the CTP mode is visible. (j−l) Spatial distribution of the CTP plasmon mode for the different welding geometries plotted in the energy range as indicated in each map. Reproduced with permission from ACS Nano, 14, 12558–12570 (2020). Copyright © 2020 American Chemical Society

SUMMARY AND OUTLOOK

The last section shows the enormous potential of pulsed laser irradiation for extending the current synthesis routes of gold NCs. By using the gained understanding of the interaction of the ultrafast laser pulses with plasmonic gold NCs, a plethora of unique morphologies could be potentially envisaged and synthesized. So far, the community has only scratched the surface and has mainly used spherical or rod-like shapes as a starting

point. However, the progress of colloidal synthesis routes in the past 20 years has opened access to a myriad of gold NCs with different shapes (e.g., cubes, triangles or wires), sizes (from 1 nm to above 200 nm), crystalline structures (single-crystalline, monotwinned or multitwinned) surface functionalization (e.g., surfactants, aminoacids, DNA, biopolymers, etc.) and dispersed in different media such as water, chloroform or hexane.[89–91] These shapes offer a large playground for laser modification and the creation of nanostructures that are not attainable by classical synthesis routes. Moreover, simulation techniques such as molecular dynamics could support the rational design of such unprecedented morphologies, as discussed above. In addition, pulsed laser excitation should be considered a viable tool to be exploited *during* the synthesis process and not only as a post-processing modification tool. It is, for example, conceivable to locally alter heat dissipation and hence cooling rates within a growing NC by smart ligand engineering or by exploiting ultrafast electron-phonon coupling, resulting in the direct translation of plasmonic to thermal local hot spots, as observed for some transition metal nitrides.[92] Under pulsed laser excitation, different parts of the NC would then reshape differently, which would result in entirely different shapes, as would be achievable by conventional synthesis routes.

Next to morphological tuning, pulsed laser excitation is extremely valuable for crystallinity and surface engineering, two critical parameters in heterogeneous catalysis. Many catalytic reactions significantly benefit from undercoordinated surface atoms, stacking faults, and other defects.[93–95] Moreover, the presence of defects involves an increase in the lattice strain that modifies the electronic structure of the NCs and, thereby, their catalytic behavior. In this sense, pulsed laser irradiation provides means to control lattice strain and the surface of gold NCs at the nanoscale as the characteristic ultrafast heating and cooling dynamic associated with the excitation of plasmonic NCs with ultrafast laser pulses facilitates the introduction of crystalline defects such as stacking faults and grain boundaries.[43]

The same discussion holds for other plasmonic materials besides gold. For example, metal NCs such as silver, copper, platinum or aluminum present remarkable plasmonic properties and can be rationally synthesized via colloidal routes.[90,91,96–101] For instance, one can imagine that femtosecond pulsed laser irradiation can be utilized to narrow the plasmon band of silver and copper NRs, according to a process similar to that observed for gold NRs. Colloidal NCs such as Al:ZnO, In_2O_3 or and $WO_{3-x,}$ and $Cu_{2-x}E$ (E = S, Se, Te) are also plasmonic. [90,91,96–102] Ultrafast laser irradiation could be applied to induce shape changes or modify the nature and distribution of defects, which would eventually affect their plasmonic and electronic properties. In particular, ultrafast laser modification could be interesting for materials where synthesis routes are currently less developed or more challenging. However, laser modification can also be utilized for non-plasmonic systems such as semiconductors, which remain so far largely unexplored. First indications showed promising results as femtosecond laser irradiation led to different (morphological and chemical) modifications in CdSe/CdS NRs than thermal heating.[103] Such an unexplored area of research, at the interface between ultrafast pulsed laser technology and colloidal synthesis routes of NCs, holds appealing prospects for the fabrication of nanomaterials with distinct physicochemical features suitable for nanotechnology.

So far, we have mainly discussed morphological and structural pulsed laser-assisted tuning of NCs. However, pulsed laser modification can also be used for elemental distribution engineering in multicomponent systems. For example, multistep synthesis methods enable the growth of multielemental plasmonic NCs such as core-shell and Janus NCs.[90,104,105] In this scenario, the extreme temperatures achieved by the lattice of plasmonic metal NCs after ultrashort pulsed laser irradiation could be utilized to fabricate partially or fully alloyed NCs. Indeed, this concept has been recently demonstrated for colloidal core-shell gold@silver NRs irradiated with 50 fs laser pulses.[106] First, the dimension and composition of gold@silver NRs were carefully controlled to obtain a longitudinal LSPR band at 800 nm, in resonance with the wavelength of the Ti:Sapphire laser (Figure 7a). Then, by irradiation at different pulse fluences, an array of effects on the shape and degree of alloying was effectively induced. At low pulse fluence, 0.32 mJ cm^{-2}, NRs with hot-dog-like morphology were obtained due to the removal of silver from the tips (Figure 7b,e,f). At intermediate fluences, 0.64 mJ/cm^{-2}, partially alloyed structures with rice-like morphology were formed (Figure 7c,g,h). Complete formation of alloyed NCs with a spherical morphology was finally attained at a fluence of 0.92 mJ·cm^{-2} (Figure 7d). These results demonstrate the potential of femtosecond pulsed laser irradiation to fabricate (partially) alloyed NCs in the liquid phase at room temperature and with precise control over their size and composition. Remarkably, this strategy should be applicable to any colloidal multimetallic heterostructures capable of absorbing laser light (i.e., by excitation of LSPRs or interband transitions). Due to the highly out-of-equilibrium processes, it is also feasible that this strategy can serve to (partially) alloy components that are classically non-miscible.

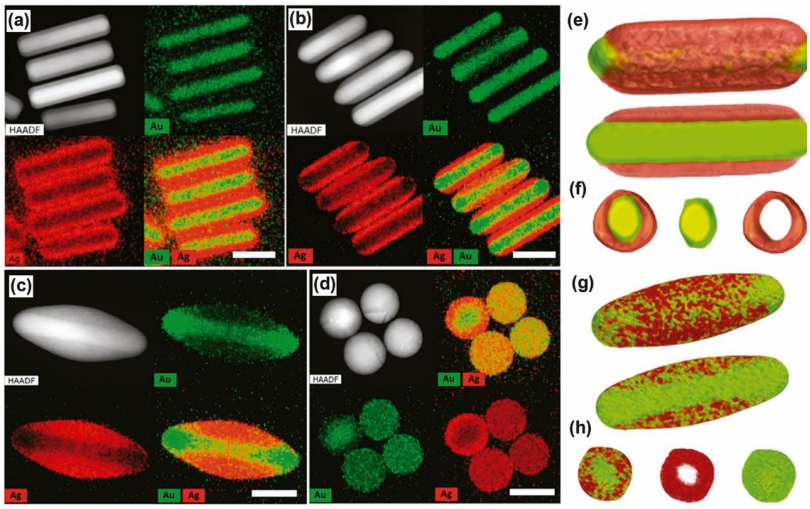

Figure 7: Elemental redistribution in bimetallic gold@silver NRs through femtosecond laser excitation. (a-d) HAADF-STEM images (top left) and quantified EDX maps (top right and bottom) of gold@silver NRs (a) irradiated with 0.32 mJ cm^{-2} (b), 0.64 mJ cm^{-2}(c), 92 mJ cm^{-2}(d) fs-laser pulses. (e-h) EDX tomography visualization (e and g, top) and their longitudinal (e and g, bottom) and transversal sections (f and h) of gold@silver NRs irradiated with 3.2 mJ cm^{-2} (e,f), and 6.4 mJ cm^{-2}(g,h) fs-laser pulses. Scale bars: 50 nm. Reproduced

with permission from Adv. Optical Mater. 9, 2002134. (2021) Copyright 2021 Wiley-VCH GmbH.

In practice, elemental distribution tuning is also highly desirable for the development of multimetallic nanocatalysts, which are the focus of intense research for green technologies.[107–111] The activity, selectivity, and stability of metal catalysts strongly depend on the interplay between their size, shape, composition, atomic distribution (mixed or segregated), and crystallinity (single vs. polycrystalline), which are all parameters that can be tuned via ultrafast pulsed laser irradiation.[112,113] For example, in bimetallic gold-palladium NRs, fs laser irradiation was shown to induce atomic redistribution of the palladium atoms and thereby enhanced its photocurrent response in a photochemical setup by 2-fold compared to the initial non-alloyed NRs.[114] Rigid coatings such as the discussed mesoporous silica shell can then be utilized to ensure the stabilization of specific anisotropic morphologies allowing for elemental and crystallinity tuning while preserving the desired morphology.[115]

Finally, it is worth noting that the envisaged exploitation of pulsed laser irradiation potential for morphology, crystallinity, surface, and atomic distribution engineering of nanomaterials requires us to continue improving our understanding of the underlying light-matter interactions. In this regard, single particle analysis combining light excitation with structural characterization is highly valuable.[116] Moreover, comprehension of atomic redistributions and defect engineering demands high-resolution structural and compositional analysis. Toward this end, looking at pulsed laser-induced processes inside the transmission electron microscope is the next challenging step. Initial experiments promise significant progress in that direction.[116] For example, Matsumura and co-workers monitored the atomic reorganization of gold NRs upon one nanosecond pulse at a time inside a high-voltage TEM,[117] while Voss et al. observed the Coulomb fission of spherical gold NCs encapsulated in a silica shell under femtosecond laser excitation inside the TEM (Figure 2d).[48] In addition, the recent developments in ultrafast TEM bring us closer to observing these effects with high time resolution,[118,119] which carries exciting prospects as it likely enables the extraction of (ultrafast) diffusion dynamics,[120,121] similar to what has been achieved for thermal heating.[38,122]

ACKNOWLEDGEMENTS

G.G.-R. acknowledges the Deutsche Forschungsgemeinschaft (GO 3526/1-1) for financial support. This work is part of the research program of AMOLF, which is partly financed by the Dutch Research Council (NWO).

AUTHOR DECLARATIONS

Conflict of interest

The authors have no conflicts to disclose.

Author contributions

Guillermo González-Rubio: Conceptualization (equal); Writing – original draft (equal); Writing – review and editing (equal). **Wiebke Albrecht**: Conceptualization (equal); Writing – original draft (equal); Writing – review and editing (equal).

DATA AVAILABILITY

Data sharing is not applicable to this article as no new data were created or analyzed.

REFERENCES

[1] S.D. Brorson, J.G. Fujimoto, and E.P. Ippen, Physical Review Letters **59**, 1962 (1987).
[2] R.W. Schoenlein, W.Z. Lin, J.G. Fujimoto, and G.L. Eesley, Physical Review Letters **58**, 1680 (1987).
[3] H.E. Elsayed-Ali, T. Juhasz, G.O. Smith, and W.E. Bron, Physical Review B **43**, 4488 (1991).
[4] S.A. Maier, *Plasmonics : Fundamentals and Applications* (Springer Science & Business Media, 2007).
[5] A.R. Rastinehad, H. Anastos, E. Wajswol, J.S. Winoker, J.P. Sfakianos, S.K. Doppalapudi, M.R. Carrick, C.J. Knauer, B. Taouli, S.C. Lewis, A.K. Tewari, J.A. Schwartz, S.E. Canfield, A.K. George, J.L. West, and N.J. Halas, Proceedings of the National Academy of Sciences of the United States of America **116**, 18590 (2019).
[6] G. Bodelón, V. Montes-García, V. López-Puente, E.H. Hill, C. Hamon, M.N. Sanz-Ortiz, S. Rodal-Cedeira, C. Costas, S. Celiksoy, I. Pérez-Juste, L. Scarabelli, A. La Porta, J. Pérez-Juste, I. Pastoriza-Santos, and L.M. Liz-Marzán, Nature Materials **15**, 1203 (2016).
[7] C. Han, M.-Y. Qi, Z.-R. Tang, J. Gong, and Y.-J. Xu, Nano Today **27**, 48 (2019).
[8] J. Zheng, X. Cheng, H. Zhang, X. Bai, R. Ai, L. Shao, and J. Wang, Chemical Reviews **121**, 13342 (2021).
[9] V. Myroshnychenko, J. Rodríguez-Fernández, I. Pastoriza-Santos, A.M. Funston, C. Novo, P. Mulvaney, L.M. Liz-Marzán, and F.J. García de Abajo, Chemical Society Reviews **37**, 1792 (2008).
[10] K. Park, S. Biswas, S. Kanel, D. Nepal, and R.A. Vaia, Journal of Physical Chemistry C **118**, 5918 (2014).
[11] G. González-Rubio, V. Kumar, P. Llombart, P. Díaz-Núñez, E. Bladt, T. Altantzis, S. Bals, O. Peña-Rodríguez, E.G. Noya, L.G. MacDowell, A. Guerrero-Martínez, and L.M. Liz-Marzán, ACS Nano **13**, 4424 (2019).
[12] X. Ye, C. Zheng, J. Chen, Y. Gao, and C.B. Murray, Nano Lett. **13**, 765 (2013).
[13] F. Kim, K. Sohn, J. Wu, and J. Huang, Journal of the American Chemical Society **130**, 14442 (2008).
[14] C. V. Shank and E.P. Ippen, Applied Physics Letters **24**, 373 (1974).
[15] T.S. Ahmadi, S.L. Logunov, and M.A. El-Sayed, Journal of Physical Chemistry **100**, 8053 (1996).
[16] P. V. Kamat, M. Flumiani, and G. V. Hartland, Journal of Physical Chemistry B **102**, 3123 (1998).
[17] S.L. Logunov, T.S. Ahmadi, M.A. El-Sayed, J.T. Khoury, and R.L. Whetten, Journal of Physical Chemistry B **101**, 3713 (1997).
[18] A. Takami, H. Kurita, and S. Koda, The Journal of Physical Chemistry B **103**, 1226 (1999).
[19] S. Link, C. Burda, B. Nikoobakht, and M.A. El-Sayed, The Journal of Physical Chemistry B **104**, 6152 (2000).
[20] H. Kurita, A. Takami, and S. Koda, Applied Physics Letters **72**, 789 (1998).
[21] S. Link, Z.L. Wang, and M.A. El-Sayed, J. Phys. Chem. B **104**, 7867 (2000).
[22] S. Link, C. Burda, M.B. Mohamed, B. Nikoobakht, and M.A. El-Sayed, The Journal of Physical Chemistry A **103**, 1165 (1999).
[23] S. Link and M.A. El-Sayed, Journal of Physical Chemistry B **103**, 8410 (1999).
[24] G. González-Rubio, T. Milagres De Oliveira, W. Albrecht, P. Díaz-Núñez, J.C. Castro-Palacio, A. Prada, R.I. González, L. Scarabelli, L. Bañares, A. Rivera, L.M. Liz-Marzán, O. Peña-Rodríguez, S. Bals, and A. Guerrero-Martínez, Journal of Physical Chemistry Letters **11**, 670 (2020).
[25] G. González-Rubio, P. Díaz-Núñez, A. Rivera, A. Prada, G. Tardajos, J. González-Izquierdo, L. Bañares, P. Llombart, L.G. Macdowell, M.A. Palafox, L.M. Liz-Marzán, O. Peña-Rodríguez, and A. Guerrero-Martínez, Science **358**, 640 (2017).

[26] G. González-Rubio, A. Guerrero-Martínez, and L.M. Liz-Marzán, Accounts of Chemical Research **49**, 678 (2016).
[27] W. Albrecht, T.-S. Deng, B. Goris, M.A. van Huis, S. Bals, and A. van Blaaderen, (2016).
[28] O. Ekici, R.K. Harrison, N.J. Durr, D.S. Eversole, M. Lee, and A. Ben-Yakar, J. Phys. D: Appl. Phys. **41**, 185501 (2008).
[29] H. Petrova, J. Perez Juste, I. Pastoriza-Santos, G. V Hartland, L.M. Liz-Marzán, and P. Mulvaney, Physical Chemistry Chemical Physics : PCCP **8**, 814 (2006).
[30] A. Plech, S. Ibrahimkutty, S. Reich, and G. Newby, Nanoscale **9**, 17284 (2017).
[31] K. Setoura, Y. Okada, and S. Hashimoto, Physical Chemistry Chemical Physics **16**, 26938 (2014).
[32] S. Wang and T. Ding, ACS Nano **13**, 32 (2019).
[33] W. Albrecht, E. Bladt, H. Vanrompay, J.D. Smith, S.E. Skrabalak, and S. Bals, ACS Nano **13**, 6522 (2019).
[34] Y. Liu, E.N. Mills, and R.J. Composto, Journal of Materials Chemistry **19**, 2704 (2009).
[35] W. Albrecht, A. van de Glind, H. Yoshida, Y. Isozaki, A. Imhof, A. van Blaaderen, P.E. de Jongh, K.P. de Jong, J. Zečević, and S. Takeda, Ultramicroscopy **193**, 97 (2018).
[36] C.M. Tollan, R. Marcilla, J.A. Pomposo, J. Rodriguez, J. Aizpurua, J. Molina, and D. Mecerreyes, ACS Applied Materials and Interfaces **1**, 348 (2009).
[37] A. Plech, R. Cerna, V. Kotaidis, F. Hudert, A. Bartels, and T. Dekorsy, Nano Letters **7**, 1026 (2007).
[38] H. Vanrompay, E. Bladt, W. Albrecht, A. Béché, M. Zakhozheva, A. Sánchez-Iglesias, L.M. Liz-Marzán, and S. Bals, Nanoscale **10**, 22792 (2018).
[39] A.B. Taylor, A.M. Siddiquee, and J.W.M. Chon, ACS Nano **8**, 12071 (2014).
[40] D. Werner and S. Hashimoto, J. Phys. Chem. C **115**, 5063 (2011).
[41] G. Baffou and R. Quidant, Laser Photonics Rev **7**, 171 (2013).
[42] G. Baffou, R. Quidant, and C. Girard, Appl. Phys. Lett. **94**, 153109 (2009).
[43] W. Albrecht, E. Arslan Irmak, T. Altantzis, A. Pedrazo-Tardajos, A. Skorikov, T.S. Deng, J.E.S. van der Hoeven, A. van Blaaderen, S. Van Aert, and S. Bals, Advanced Materials **33**, 2100972 (2021).
[44] A. Pyatenko, H. Wang, N. Koshizaki, and T. Tsuji, Laser and Photonics Reviews **7**, 596 (2013).
[45] A. Plech, V. Kotaidis, M. Lorenc, and J. Boneberg, Nature Phys **2**, 44 (2006).
[46] A. Plech, P. Leiderer, and J. Boneberg, Laser & Photonics Reviews **3**, 435 (2009).
[47] D. Werner, A. Furube, T. Okamoto, and S. Hashimoto, J. Phys. Chem. C **115**, 8503 (2011).
[48] J.M. Voss, P.K. Olshin, R. Charbonnier, M. Drabbels, and U.J. Lorenz, ACS Nano **13**, 12445 (2019).
[49] G. Bongiovanni, P.K. Olshin, C. Yan, J.M. Voss, M. Drabbels, and U.J. Lorenz, Nanoscale Adv. **3**, 5277 (2021).
[50] A. Pyatenko, M. Yamaguchi, and M. Suzuki, J. Phys. Chem. C **113**, 9078 (2009).
[51] K. Yamada, K. Miyajima, and F. Mafuné, J. Phys. Chem. C **111**, 11246 (2007).
[52] M. Shoji, K. Miyajima, and F. Mafuné, J. Phys. Chem. C **112**, 1929 (2008).
[53] L. Delfour and T.E. Itina, J. Phys. Chem. C **119**, 13893 (2015).
[54] S. Inasawa, M. Sugiyama, and Y. Yamaguchi, Journal of Physical Chemistry B **109**, 3104 (2005).
[55] D. Luo, C. Yan, and T. Wang, Small **11**, 5984 (2015).
[56] C.A.S. Batista, R.G. Larson, and N.A. Kotov, Science **350**, 1242477 (2015).
[57] Y. Min, M. Akbulut, K. Kristiansen, Y. Golan, and J. Israelachvili, Nature Materials **7**, 527 (2008).
[58] M.A. Boles, M. Engel, and D. V. Talapin, Chemical Reviews **116**, 11220 (2016).
[59] A. Heuer-Jungemann, N. Feliu, I. Bakaimi, M. Hamaly, A. Alkilany, I. Chakraborty, A. Masood, M.F. Casula, A. Kostopoulou, E. Oh, K. Susumu, M.H. Stewart, I.L. Medintz, E. Stratakis, W.J. Parak, and A.G. Kanaras, Chemical Reviews **119**, 4819 (2019).

[60] J.S. Suk, Q. Xu, N. Kim, J. Hanes, and L.M. Ensign, Advanced Drug Delivery Reviews **99**, 28 (2016).
[61] S. Mourdikoudis and L.M. Liz-Marzán, Chemistry of Materials **25**, 1465 (2013).
[62] G. González-Rubio, L. Scarabelli, A. Guerrero-Martínez, and L.M. Liz-Marzán, ChemNanoMat **6**, 698 (2020).
[63] A. Guerrero-Martínez, J. Pérez-Juste, and L.M. Liz-Marzán, Advanced Materials **22**, 1182 (2010).
[64] C. Hanske, M.N. Sanz-Ortiz, and L.M. Liz-Marzán, Advanced Materials **30**, 1707003 (2018).
[65] W.M. Haynes, D.R. Lide, and T.J. Bruno, *CRC Handbook of Chemstry and Physics*, 97th ed. (CRC Press, 2016).
[66] J. Huang, J. Park, W. Wang, C.J. Murphy, and D.G. Cahill, ACS Nano **7**, 589 (2013).
[67] S.C. Nguyen, Q. Zhang, K. Manthiram, X. Ye, J.P. Lomont, C.B. Harris, H. Weller, and A.P. Alivisatos, ACS Nano **10**, 2144 (2016).
[68] H. Yun, Y.J. Lee, M. Xu, D.C. Lee, G.E. Stein, and B.J. Kim, ACS Nano **14**, 9644 (2020).
[69] H. Yun, J.W. Yu, Y.J. Lee, J.-S. Kim, C.H. Park, C. Nam, J. Han, T.-Y. Heo, S.-H. Choi, D.C. Lee, W.B. Lee, G.E. Stein, and B.J. Kim, Chem. Mater. **31**, 5264 (2019).
[70] P. Díaz-Núñez, G. González-Rubio, A. Prada, J. González Izquierdo, A. Rivera, L. Bañares, A. Guerrero-Martínez, and O. Peña-Rodríguez, Journal of Physical Chemistry C **122**, 19816 (2018).
[71] W. Albrecht, E. Bladt, H. Vanrompay, J.D. Smith, S.E. Skrabalak, and S. Bals, ACS Nano **13**, 6522 (2019).
[72] H. Cho, J.W. Shin, and R. Ryoo, The Journal of Physical Chemistry C **124**, 12855 (2020).
[73] G. González-Rubio, J. Mosquera, V. Kumar, A. Pedrazo-Tardajos, P. Llombart, D.M. Solís, I. Lobato, E.G. Noya, A. Guerrero-Martínez, J.M. Taboada, F. Obelleiro, L.G. MacDowell, S. Bals, and L.M. Liz-Marzán, Science **368**, 1472 (2020).
[74] T. Altantzis, I. Lobato, A. De Backer, A. Béché, Y. Zhang, S. Basak, M. Porcu, Q. Xu, A. Sánchez-Iglesias, L.M. Liz-Marzán, G. Van Tendeloo, S. Van Aert, and S. Bals, Nano Letters **19**, 477 (2019).
[75] W. Albrecht and S. Bals, The Journal of Physical Chemistry C **124**, 27276 (2020).
[76] W. Albrecht, S. Van Aert, and S. Bals, Accounts of Chemical Research **54**, 1189 (2021).
[77] B. Goris, J. De Beenhouwer, A. De Backer, D. Zanaga, K.J. Batenburg, A. Sánchez-Iglesias, L.M. Liz-Marzán, S. Van Aert, S. Bals, J. Sijbers, and G. Van Tendeloo, Nano Letters **15**, 6996 (2015).
[78] M.C. Scott, C.C. Chen, M. Mecklenburg, C. Zhu, R. Xu, P. Ercius, U. Dahmen, B.C. Regan, and J. Miao, Nature **483**, 444 (2012).
[79] B. Goris, S. Bals, W. Van den Broek, E. Carbó-Argibay, S. Gómez-Graña, L.M. Liz-Marzán, and G. Van Tendeloo, Nature Materials **11**, 930 (2012).
[80] C.C. Chen, C. Zhu, E.R. White, C.Y. Chiu, M.C. Scott, B.C. Regan, L.D. Marks, Y. Huang, and J. Miao, Nature **496**, 74 (2013).
[81] Z. Qin, T. Du, Y. Zheng, P. Luo, J. Zhang, M. Xie, Y. Zhang, Y. Du, L. Yin, D. Cui, Q. Lu, M. Lu, X. Wang, and H. Jiang, Small **15**, 1902755 (2019).
[82] K. Cai, W. Zhang, J. Zhang, H. Li, H. Han, and T. Zhai, ACS Applied Materials and Interfaces **10**, 36703 (2018).
[83] Y. Ihm, D.H. Cho, D. Sung, D. Nam, C. Jung, T. Sato, S. Kim, J. Park, S. Kim, M. Gallagher-Jones, Y. Kim, R. Xu, S. Owada, J.H. Shim, K. Tono, M. Yabashi, T. Ishikawa, J. Miao, D.Y. Noh, and C. Song, Nature Communications **10**, (2019).
[84] G.M. Whitesides and B. Grzybowski, Science **295**, 2418 (2002).
[85] M. Grzelczak, J. Vermant, E.M. Furst, and L.M. Liz-Marzan, ACS Nano **4**, 3591 (2010).
[86] G. González-Rubio, J. González-Izquierdo, L. Bañares, G. Tardajos, A. Rivera, T. Altantzis, S. Bals, O. Peña-Rodríguez, A. Guerrero-Martínez, and L.M. Liz-Marzán, Nano Letters **15**, 8282 (2015).
[87] N.J. Halas, S. Lal, W.-S. Chang, S. Link, and P. Nordlander, Chemical Reviews **111**, 3913 (2011).

[88] T.M. De Oliveira, W. Albrecht, G. González-Rubio, T. Altantzis, I.P.L. Hoyos, A. Béché, A. Guerrero-Martínez, L.M. Liz-Marzán, and S. Bals, ACS Nano **14**, 12558 (2020).
[89] M. Ha, J.H. Kim, M. You, Q. Li, C. Fan, and J.M. Nam, Chemical Reviews **119**, 12208 (2019).
[90] Y. Xia, K.D. Gilroy, H.C. Peng, and X. Xia, Angewandte Chemie - International Edition **56**, 60 (2017).
[91] F. Fievet, S. Ammar-Merah, R. Brayner, F. Chau, M. Giraud, F. Mammeri, J. Peron, J.-Y. Piquemal, L. Sicard, and G. Viau, Chemical Society Reviews **47**, 5187 (2018).
[92] S.H.C. Askes and E.C. Garnett, Advanced Materials **33**, 2105192 (2021).
[93] L. Dubau, J. Nelayah, S. Moldovan, O. Ersen, P. Bordet, J. Drnec, T. Asset, R. Chattot, and F. Maillard, ACS Catalysis **6**, 4673 (2016).
[94] Y. Jia, K. Jiang, H. Wang, and X. Yao, Chem **5**, 1371 (2019).
[95] Z. Li, J.-Y. Fu, Y. Feng, C.-K. Dong, H. Liu, and X.-W. Du, Nature Catalysis **2**, 1107 (2019).
[96] A. Agrawal, S.H. Cho, O. Zandi, S. Ghosh, R.W. Johns, and D.J. Milliron, Chemical Reviews **118**, 3121 (2018).
[97] S. Lu, H. Yu, S. Gottheim, H. Gao, C.J. Desantis, B.D. Clark, J. Yang, C.R. Jacobson, Z. Lu, P. Nordlander, N.J. Halas, and K. Liu, Journal of the American Chemical Society **140**, 15412 (2018).
[98] O. Peña-Rodríguez, P. Díaz-Núñez, G. González-Rubio, V. Manzaneda-González, A. Rivera, J.M. Perlado, E. Junquera, and A. Guerrero-Martínez, Scientific Reports **10**, 5921 (2020).
[99] L.M. Liz-Marzán, Langmuir **22**, 32 (2006).
[100] S.E. Lohse, N.D. Burrows, L. Scarabelli, L.M. Liz-Marzán, and C.J. Murphy, Chemistry of Materials **26**, 34 (2014).
[101] S. Kim, J.-M. Kim, J.E. Park, and J.-M. Nam, Advanced Materials **30**, 1704528 (2018).
[102] R. Buonsanti, A. Llordes, S. Aloni, B.A. Helms, and D.J. Milliron, Nano Lett. **11**, 4706 (2011).
[103] W. Albrecht, B. Goris, S. Bals, E.M. Hutter, D. Vanmaekelbergh, M.A. Van Huis, and A. Van Blaaderen, Nanoscale **9**, 4810 (2017).
[104] Z. Huang, J. Gong, and Z. Nie, Accounts of Chemical Research **52**, 1125 (2019).
[105] K.D. Gilroy, A. Ruditskiy, H.-C. Peng, D. Qin, and Y. Xia, Chemical Reviews **116**, 10414 (2016).
[106] G. González-Rubio, P. Díaz-Núñez, W. Albrecht, V. Manzaneda-González, L. Bañares, A. Rivera, L.M. Liz-Marzán, O. Peña-Rodríguez, S. Bals, and A. Guerrero-Martínez, Advanced Optical Materials **9**, 2002134 (2021).
[107] M. Luo and S. Guo, Nature Reviews Materials **2**, 17059 (2017).
[108] Y. Sun and S. Dai, Science Advances **7**, eabg1600 (2021).
[109] P.-C. Chen, X. Liu, J.L. Hedrick, Z. Xie, S. Wang, Q.-Y. Lin, M.C. Hersam, V.P. Dravid, and C.A. Mirkin, Science **352**, 1565 (2016).
[110] M.B. Ross, P. De Luna, Y. Li, C.-T. Dinh, D. Kim, P. Yang, and E.H. Sargent, Nature Catalysis **2**, 648 (2019).
[111] Y. Li, Y. Sun, Y. Qin, W. Zhang, L. Wang, M. Luo, H. Yang, and S. Guo, Advanced Energy Materials **10**, 1903120 (2020).
[112] M. Zhou, C. Li, and J. Fang, Chemical Reviews **121**, 736 (2021).
[113] Y. Shi, Z. Lyu, M. Zhao, R. Chen, Q.N. Nguyen, and Y. Xia, Chemical Reviews **121**, 649 (2021).
[114] M. Nazemi, S.R. Panikkanvalappil, C.-K. Liao, M.A. Mahmoud, and M.A. El-Sayed, ACS Nano **15**, 10241 (2021).
[115] W. Albrecht, J.E.S. van der Hoeven, T.-S. Deng, P.E. de Jongh, and A. van Blaaderen, Nanoscale **9**, 2845 (2017).
[116] M. Dieperink, F. Scalerandi, and W. Albrecht, Nanoscale **14**, 7460 (2022).
[117] K. Aso, K. Shigematsu, T. Yamamoto, and S. Matsumura, Microscopy **68**, 174 (2019).
[118] S.A. Aseyev, E.A. Ryabov, B.N. Mironov, and A.A. Ischenko, Crystals **10**, 452 (2020).
[119] A. Feist, N. Bach, N. Rubiano da Silva, T. Danz, M. Möller, K.E. Priebe, T. Domröse, J.G. Gatzmann, S. Rost, J. Schauss, S. Strauch, R. Bormann, M. Sivis, S. Schäfer, and C. Ropers, Ultramicroscopy **176**, 63 (2017).
[120] B. Barwick and A.H. Zewail, ACS Photonics **2**, 1391 (2015).
[121] P.K. Olshin, G. Bongiovanni, M. Drabbels, and U.J. Lorenz, Nano Letters **21**, 612 (2021).

[122] A. Skorikov, W. Albrecht, E. Bladt, X. Xie, J.E.S. Van Der Hoeven, A. Van Blaaderen, S. Van Aert, and S. Bals, ACS Nano **13**, 13421 (2019).

PLEASE CITE THIS ARTICLE AS DOI: 10.1063/5.0122888

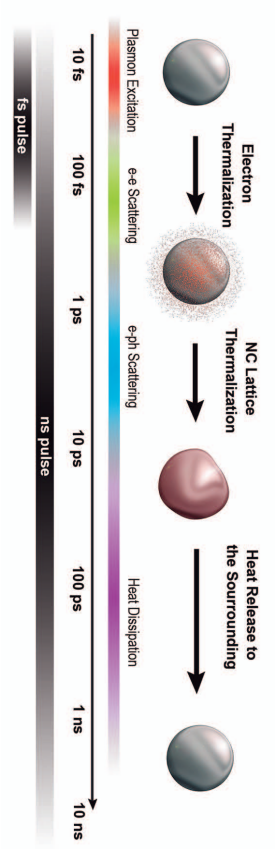

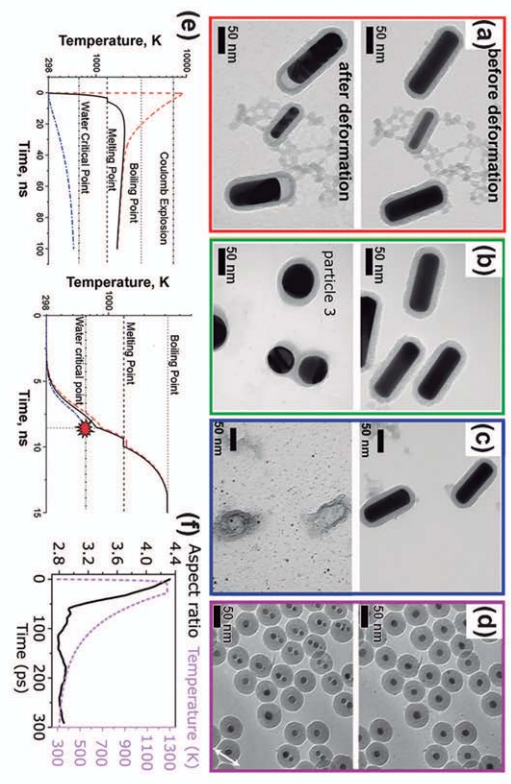

Applied Physics Letters

PLEASE CITE THIS ARTICLE AS DOI: 10.1063/5.0122888

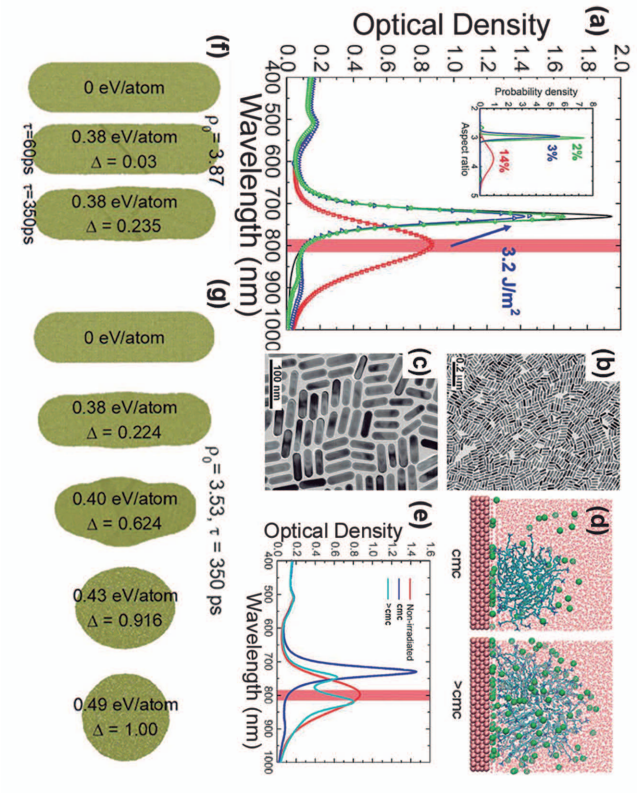

Applied Physics Letters

PLEASE CITE THIS ARTICLE AS DOI: 10.1063/5.0122888

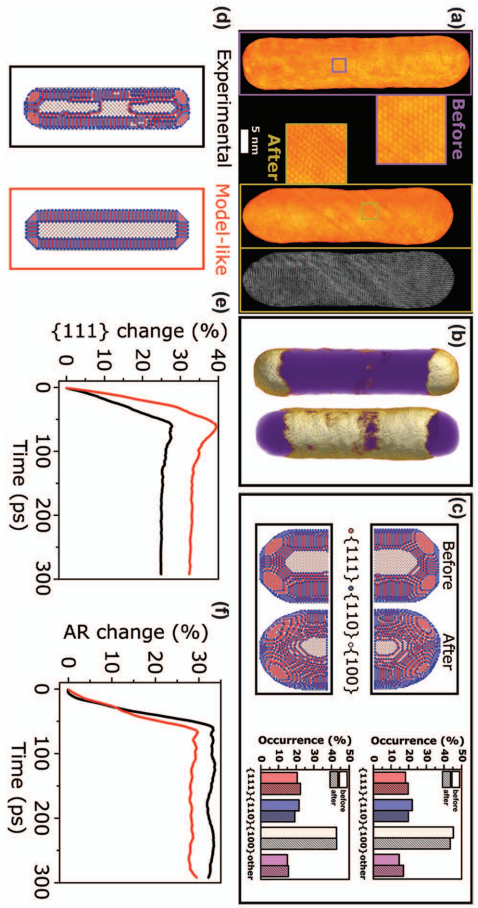

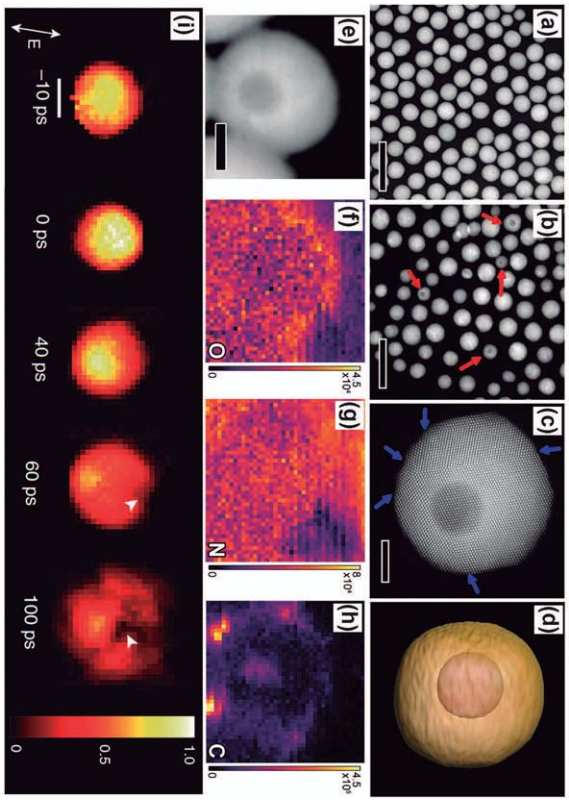

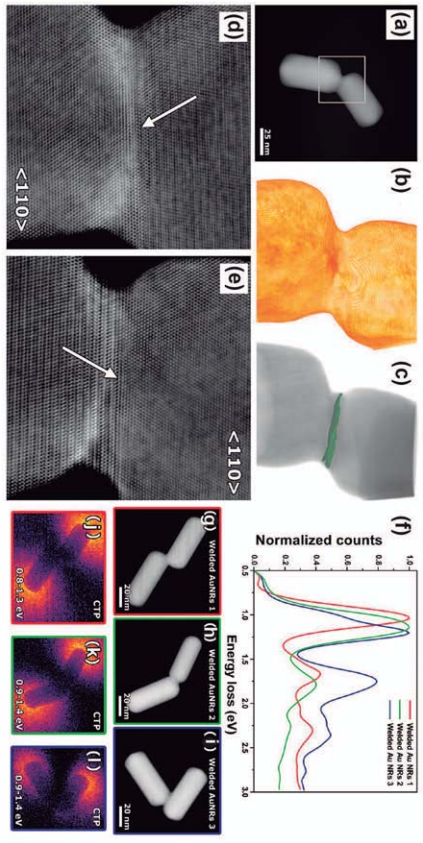

Applied Physics Letters

PLEASE CITE THIS ARTICLE AS DOI: 10.1063/5.0122888